JOURNAL OF OPTOELECTRONICS AND ADVANCED MATERIALS, Vol. 11, No. 11, November 2009, p. 1855 - 1859

Current transport mechanisms of n-ZnO/p-CuO heterojunctions

F. ÖZYURT KUŞ, T. SERİN, N. SERİN
Department of Physics Engineering, University of Ankara, 06100 Ankara, Turkey

In this study, n-ZnO/p-CuO heterojunction have been fabricated by sol-gel dip-coating technique which is simple and inexpensive. The structure of the p-CuO/n-ZnO was analyzed by X-ray diffraction spectroscopy and UV-VIS spectroscopy. The electrical junction properties were characterised by temperature dependent current-voltage (I-V) characteristics and at high frequency capacitance-voltage (C-V) characteristic at room temperature. The structure showed non-ideal behaviour of I-V characteristics with an ideality factor of 3.5 at room temperature. Temperature dependent forward current-voltage measurements suggest that trap-assisted multi-step tunnelling is the dominant current mechanism in this structure.

(Received October 15, 2009; accepted November 22, 2009)

Keywords: ZnO, CuO, Heterojunction, Sol-gel, I-V characteristics

1. Introduction

Transparent conducting oxides (TCOs) are widely used as transparent electrodes for optoelectronic devices. Zinc oxide (ZnO) is a wide direct band gap n-type semiconductor with a band gap energy of about 3.2 eV [1]. ZnO is used in many different applications such as conducting electrode in solar cell [1], gas sensor [2-8], flat panel display [9], surface-wave transducers [10] and piezoelectric devices [11].

Copper oxide (CuO) is p-type semiconductor with a band gap energy of about 1.51-1.74 eV [12-13]. CuO is especially used in solar cell technology and photovoltaic applications.

P-n junctions have been developed for various gases such as ZnO/CuO for CO and H_2 sensing [2-8, 14], CuO/SnO_2 for H_2S, C_4H_{10} and CH_2 sensing [15-16] recently.

A variety of techniques have been used to prepare heterojunction. ZnO/CuO heterojunctions have been made by the solid state synthesis route [6], pressing [8], liquid phase co-precipitation method [3] and spin coating method [2]. In this paper, a n-ZnO/p-CuO heterojunction was fabricated by sol-gel dip coating technique. Sol-gel method has several advantages in producing thin films, such as relatively homogeneous composition, easy control of the film thickness, fine microstructure and low temperature sintering.

In this paper, we describe the deposition process of n-ZnO/p-CuO heterojunction. Then the optical, structural and electrical properties of the samples were studied by the UV-VIS spectroscopy, X-ray diffraction spectroscopy, temperature dependent current-voltage and capacitance-voltage at room temperature measurements respectively. The purpose of this work is to clue the current transport mechanism of n-ZnO/p-CuO heterojunctions.

2. Experimental

In order to prepare ZnO solution, firstly, zinc acetate 2-hydrate [$Zn(CH_3COO)_2.2H_2O$] was dissolved in ethanol (CH_3COCH_3, 99.9 %, Merck) and then lactic acid was added as hydrolysis catalyst in drops. Afterwards solution was thoroughly mixed by a magnetic stirs for 2 hours, and homogeneous transparent solution was obtained which had a concentration of 0.4M. Each coating on the ATO (Antimony Tin Oxide) substrate was first dried at 250 °C for 5 min. This process of coating was repeated for 10 times and then the final film was annealed at 250 °C for 15 min.

CuO layer was deposited on ZnO. The CuO sol was prepared by adding copper II acetate ($(CH_3COO)_2Cu.H_2O$) to ethanol and mixing the both components. While sol was mixing, the triethylamine was added in the sol. After the sol prepared, the CuO film was deposited on the ZnO film was dried at 250 °C for 5 min. This process of coating was repeated for 10 times and then the p-n junction was annealed at 250 °C for 30 min.

After 10 coating for the ZnO film, thickness of the film was calculated ~70 nm and after 10 coating for the CuO film, it was calculated ~212 nm.

After ZnO/CuO heterojunction was prepared, the contact was composed between the coated film and Cu wire. To insure good contact between the film and Cu wire, Ag paste was used. The schematic band diagram of ZnO/CuO heterojunction is shown in Fig. 1.

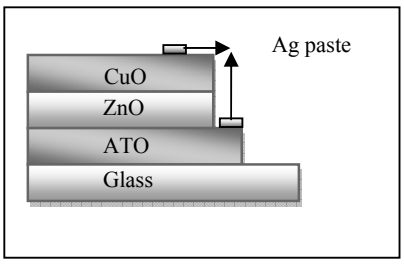

Fig. 1. The schematic diagram of ZnO/CuO heterojunction.

The crystal structure of the n-ZnO/p-CuO heterojunction was determined by XRD using Rikagu D-

max 2200 X-Ray diffractometer system with CuK_α radiation (λ=1.5405 Å) and by the UV-VIS spectroscopy (350-1100nm) using Perkin Elmer UV-VIS Spectrometer Lambda 2S. The current-voltage characteristics of the heterojunctions were measured with a system which consists of a DC voltage–current source Keithley 2420, a specially designed sample holder and computer. Thin films samples were mounted in the sample holder. To control the temperature of the samples, Lake Shore 330 autotuning temperature controller is used.

3. Results and discussion

Fig. 2 shows XRD spectrum (using 2θ values in the range of 10-90°) of n-ZnO/p-CuO heterojunction.

The peaks (002) and (100) of ZnO are located at 2θ =34.96° and 2θ =31.26° and the peaks ($11\bar{1}$) and (200) of CuO are located at 2θ =35.41° and 2θ =38.16° are the dominant and weak peak of ZnO and CuO respectively. The lattice constants of ZnO calculated from the present data are a= 3.300 Å and c= 5.131 Å which are in agreement with a= 3.253 Å and c= 5.209 Å of ZnO known from the literature (JCPDS Card No. 80-00075) and the lattice constants of CuO calculated from the present data are a= 4.774 Å, b= 3.434Å and c= 5.131 Å which are in agreement with the values a= 4.68 Å, b= 3.42 Å and c= 5.129 Å of CuO obtained by Kimura et al [17].

The band gap of ZnO and CuO were determined from measured transmittance spectra.

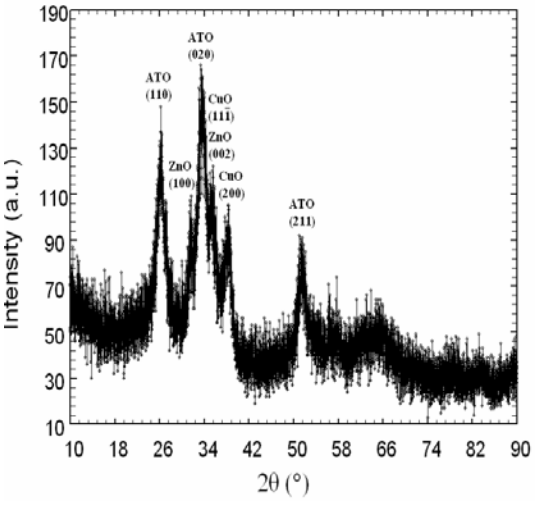

Fig. 2 XRD spectrum of a n-ZnO/p-CuO heterojunction.

Fig. 3. shows a plot of the square of the absorption coefficient (α^2) of ZnO and CuO films fabricated onto glass substrate as a function of the energy of incident radiation. For this, the fundamental absorption coefficient α was evaluated using $\alpha=\ln T^{-1}/d$ where d is the film thickness and T is the transmittance. The optical band gap, E_g, of the film was calculated using the Tauc relation, which is given as $\alpha=\alpha_o (h\nu-E_g)^n$ where hν is the photon energy, α_o is a constant and n = 0.5, 1.5, 2 or 3 for allowed direct, forbidden direct, allowed indirect and forbidden indirect electronic transitions, respectively [18]. In the present case the band-gap energy gap (E_g) has been estimated by assuming an allowed direct transition (n=1/2). The factor $(\alpha)^2$ varies linearly with hν in the high-energy region. In the low-energy region, the absorption spectrum deviates from the straight line, as shown in Fig. 3. The band gap was obtained by extrapolating the linear portion of the plot of $(\alpha)^2$ against hν to $(\alpha)^2= 0$. The intercept on energy axis gives the value of band gap energy (E_g) for the film. The band gap energy (E_g) values of ZnO and CuO are 3.3 and 1.8 eV respectively, which are in agreement with what have been reported previously [19, 13].

XRD and UV-VIS measurements showed that ZnO films consisted of hexagonal wurtzite crystal grains with energy band gap of 3.3eV. At ambient conditions, the thermodinamically stable phase is hexagonal wurtzite, the cubic zinc blende ZnO

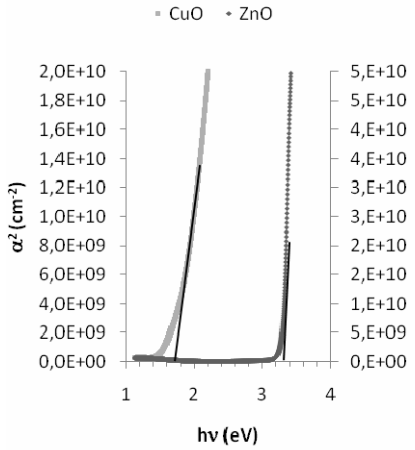

Fig. 3 Square of the absorbtion coefficient as a function of photon energy for ZnO (right axis) and CuO(left axis) films .

structure can be stabilized only by layer growth on cubic substrates, and the cubic rocksalt structure may be obtained at relatively high pressures [19]. In our heterojunctions, the ZnO films were deposited onto the ATO substrates. The ATO films are a tetragonal system because tin oxide is a tetragonal system and the lattice parameters are not affected much the incorporation of the dopants in the films [20], is hexagonal wurtzite system. The CuO layer is monoclinic system. Since all layer at our heterojunctions are different crystal systems, the lattice mismatch occur. To confirm the presence of the interface states, we calculate the lattice mismatch given by the relation [21]:

$$\frac{\Delta a}{a}=\frac{a_2-a_1}{a_2} \quad (1)$$

where a_1 and a_2 are the lattice constant of the ZnO and CuO respectively. The lattice mismatch between CuO and

ZnO calculated to be 32%, which is higher than the Cu_2O/ZnO heterojunction with the mismatch of 7.1% [22], and Cu_2O/ZnO/ITO p-i-n heterojunction with the mismatch 27.1% [23]. So the lattice mismatch leads to an interface defect states [23].

In order to determine the dominant current transport mechanism through n-ZnO/p-CuO heterojunctions, we measured the I-V characteristics at various temperatures. The forward and reverse bias I-V graphics of ZnO/CuO heterojunction samples at different temperature in the range of 300-360 K are shown in Fig. 4 (a). The sample was kept in the dark condition during the measurement. It is obvious from Fig. 4 (a) that the heterojunctions are rectifying in nature with a turn on voltage of ~0.5 V and under reverse voltages, the breakdown voltage for the sample is ~0.6 V which is same as that of ZnO/Cu_2O heterojunction prepared by RF-magnetron sputtering [24] and Cu_2O/ZnO/ITO p-i-n heterojunction prepared by electrochemical deposition method [23].

The current at real diode were given at Eq. (2)

$$I = I_0 \exp\left(\frac{qV}{nkT}\right)\left[1 - \exp\left(-\frac{qV}{kT}\right)\right] \qquad (2)$$

where q is electronic charge, I_0 is the reverse saturation current, V is the applied voltage, n is ideality factor, k is Boltzman constant and T is temperature.

For $\mathbf{V} > 3\mathbf{kT}/\mathbf{q}$, Eq. (2) can also be shown as

$$I = I_0 \exp\left(\frac{qV}{nkT}\right) \qquad (3)$$

The ideality factor (n) is obtained from the slope of the plot lnI versus V. The forward bias ln (I)-V characteristics of the samples at different temperature in the range of 300-360 K are given in Fig. 4 (b). The forward current can be classified into two regions. In the region II, the forward currents behave linearly due to the serial resistance effect on the system. In region I, the forward current can be expressed by:

$$I = I_0 \exp(AV) \qquad (4)$$

There are three models for explaining the current through heterojunctions: (1) A is independent of the measuring temperature T for a tunnelling model, (2) A is temperature dependent, n=1, A=q/kT for the diffusion model, (3) A is temperature dependent, n=2, A=q/2kT for the recombination model [25, 26].

The ideality factor (n), the reverse saturation current I_0 (which is a function of temperature, depending on the nature of dominant carrier transport mechanisms in the heterojunction [25]) and the slope of ln (I)-V graphics A (is independent of the voltage) of the samples are calculated from the graphics in Fig. 4 (b) and shown in Table 1.

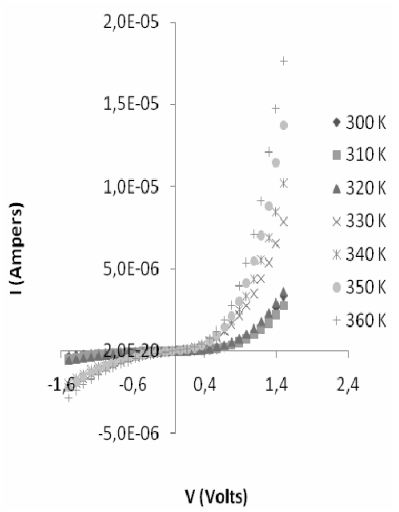

(a)

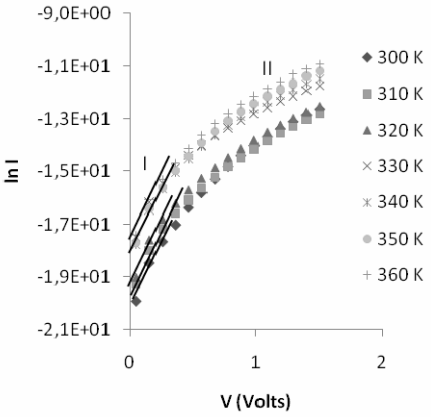

(b)

Fig. 4 Current-voltage characteristics of n-ZnO/p-CuO heterojunction at various temperature in the dark shown in (a) linear and (b) logarithmic scales.

In Table 1, the slope A of the ln (I)-V graphics is temperature insensitive. Therefore, the data are consistent with Eq. (4). The ideality factor n is larger than 2.

The temperature dependence of the current at constant voltage is shown in Fig. 5. According to the curve which is related to the formula lnI=aT+bV, the current transport mechanism is a multi-step tunnelling [27].

Table 1. The I_0, A and n values for the sample of the n-ZnO/p-CuO heterojunction

T (K)	I_0 (A)	A (V^{-1})	n
300	1.39×10^{-9}	11.0	3.5
310	2.80×10^{-9}	10.1	3.7
320	2.80×10^{-9}	10.6	3.4
330	1.75×10^{-9}	9.7	3.6
340	1.26×10^{-9}	10.1	3.4
350	1.37×10^{-9}	10.0	3.3
360	1.84×10^{-9}	10.1	3.2

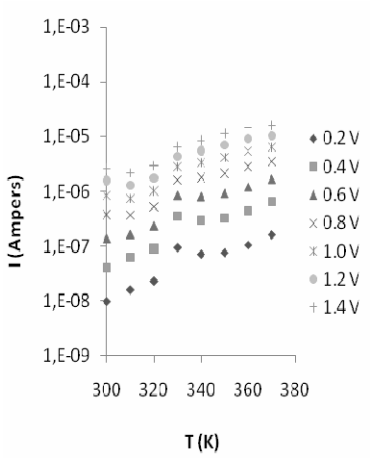

Fig. 5 The dark current versus temperature at constant voltage.

The temperature dependence of saturation current I_0 is expressed as:

$$I_0 = I_{00} \exp\left(-\frac{\Delta E_a}{kT}\right) \tag{5}$$

where ΔE_a is the thermal activation energy of carrier conduction. From the slopes of ln (I_0) versus T^{-1} graphics illustrated in Fig. 6, the activation energy was calculated to be 0.412 eV. The data fits almost on straight lines, which agrees with the multi-step tunnelling model.
The capacitance per unit area given by Anderson [28]

$$C = \left\{\frac{q\varepsilon_n\varepsilon_p N_a N_d}{2\left(\varepsilon_n N_d + \varepsilon_p \varepsilon_a\right)}\right\}\left(V_{bi} - V\right)^{-1/2} \tag{6}$$

where ε_n ,ε_p are the dielectric constant and N_d ,N_a are ionized impurity density of ZnO and CuO respectively, V_{bi} is the built in potential and V is the applied voltage.

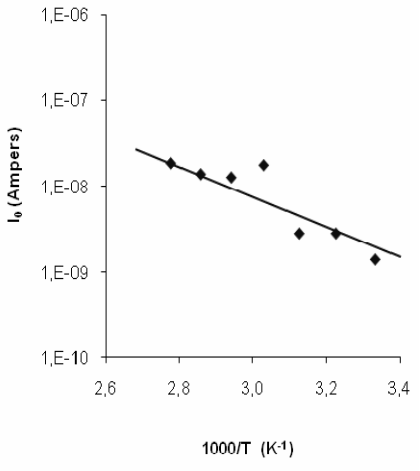

Fig. 6 The dark current pre-exponential term versus T^{-1}.

The capacitance-voltage characteristics of n-ZnO /p-CuO heterojunction at 1 MHz frequency in dark and at room temperature is shown in Fig. 7. The straight lines extrapolated to $1/C^2$=0 gives the value of built-in potential V_{bi}, 1.5 eV, which is agreement with previously published the value for ZnO/Si heterojunctions 1.49 eV [29] and rather great previously published the value for ZnO:Al/n-Si heterojunctions 0.56 eV [25]. The built-in potential 1.5 eV much larger than the activation energy of the saturation current 0.412 eV confirmed the tunnelling model. The turn on voltage of this heterojunction is much smaller than the built-in potential, this is also confirmed the tunneling model. The slope of $1/C^2$-V line gives the value of N_d. For the data shown in Fig. 7 the corresponding value is 2.87×10^{12} cm^{-3}.

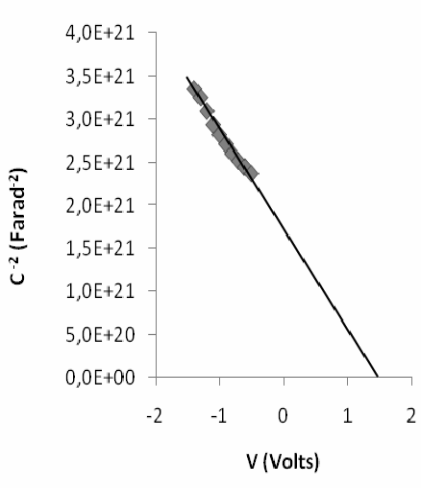

Fig.7 C^{-2} versus V plots of n-ZnO /p-CuO heterojunctions measured at 1 MHz in dark.

4. Conclusion

n-ZnO/p-CuO heterojunctions have been successfully fabricated onto ATO substrates using sol-gel dip coating method. The thickness of ZnO film prepared by 10 times coating is ~70 nm while that of CuO film coated 10 times is ~212 nm. At room temperature, the diode turn-on voltage is of ~0.5V. The temperature dependent I-V characteristics of the n-ZnO/p-CuO heterojunction showed that the forward current transport can be explained with a multi-step tunnelling model between 300 and 360 K. While the activation energy of the saturation current is about 0.412 eV, the built-in potential is about 1.5 eV.

Acknowledgements

This study was supported by Grant No. 20070745054 from Bilimsel Araştırma Projeleri (BAP) (Scientific Research Projects Department) at Ankara University.

References

[1] D. G. Baik, S. M. Cho, Thin Solid Films **354,** 227 (1999).
[2] H. Y. Bae, G. M. Choi, Sens. Actuators B **55,** 47 (1999).
[3] Y. Hu, X. Zhou, Q. Han, Q. Cao, Y. Huang, Materials Science and Engineering B **99,** 41 (2003).
[4] G. Uozumi, M. Miyayama, H. Yanagida, J. Mater. Sci. **32,** 2991 (1997).
[5] D. H. Yoon, J. H. Yu, G. M. Choi, Sens. Actuators B **46** 15 (1998).
[6] S. Aygün, D. Cann, Sens. Actuators B **106,** 837 (2005).
[7] S. Mridha, D. Basak, Semicond. Sci. Technol. **21,** 928 (2006).
[8] J. D. Choi, G. M. Choi, Sens. Actuators B **69,** 120 (2000).
[9] Z. Z. Ye, F. Yang, Y. F. Lu, M. J. Zhi, H. P. Tang, L. P. Zhu, Solid State Communications **142** 425 (2007).
[10] F. S. Hickermell, Proc. IEEE **64** 631 (1976).
[11] D. Zaouk, Y. Zaatar, R. Asmar , J. Jabbour, Microelectronics Journal **37 11** 1276 (2006).
[12] B. Balamurugan. B.R Mehta Thin Solid Films **396** 47 (2006) .
[13] A.Y.Oral, E.Menşur, M.H.Aslan, E.Başaran, Mater. Chem. Physics **83** 140 (2004).
[14] Y. Nakamura, A. Ando, T. Tsurutani, O. Okada, M. Miyamama, K. Koumuoto, H. Yanagida, Chemistry letters 413 (1986).
[15] J. Tamaki, K. Shimanoe, Y. Yamad, Y. Yamamoto, N. Miura, N. Yamazoe, Sensor and Actuators B **49,** 121(1998).
[16] X. Zhou, Q. Cao, H. Huang, Y. Hu, Materials Science and Engineering, B **99** 44 (2003).
[17] T. Kimura, Y. Sekio, H. Nakamura, T. Siegrist, P. Ramirez, Nature Materials **7** 291 (2008).
[18] J. C. Tauc, A. Menth J.Non Cryst. Solids **569,** 8-10 (1972)
[19] Ü. Özgür, Ya. I. Alivov, C. Liu, A. Teke, M. A. Reshchikov, S. Doğan, V. Avrutin, S. J. Cho, H. Morkoç, Journal of Applied Physics **98,** 041301 (2005).
[20] M. Fantini, I. Torriani, Thin Solid Films **138,** 255 (1986).
[21] Pallab Bhattacharya, Semiconductor Optoelectronic Devices, Second Edition (1997) 22.
[22] K. Akimoto, S. Izhizuka, M. Yanagita, Y. Nawa, Goutam K. Paul, T. Sakuari, Solar Energy **80,** 715 (2006).
[23] D. K. Zhang, Y. C. Liu, Y. L. Liu, H. Yang, Physica B **351,** 178 (2004).
[24] S. Ishizuka, K. Suzuki, Y. Okamoto, M. Yanagita, T. Sakurai, K. Akimoto, N. Fujiwara, H. Kobayashi, K. Matsubara and S. Niki, Phys. Stat. Sol. (C) **1(**4), 1067 (2004).
[25] D. Song, D.-H. Neuhaus, J. Xia, A.G. Aberle, Thin Solid Films **422** 180 (2002).
[26] H. Matsuura, IEEE Trans. Electron Devices **36,** 2908 (1989).
[27] A. R. Riben, D. L. Feucht, Int. J. Elektron. **20,** 583 (1966).
[28] R. L. Anderson, Solid Satate Electronics **5,** 341 (1962).
[29] Y. Zhang, J. Xu, B. Lin, Z. Fu, S. Zhong, C. Liu, Z. Zhang Applied Surface Science **252,** 3449 (2006).

*Corresponding author: figeno@hacettepe.edu.tr